NOTICE TO READER

Due to an error in original pagination by the publisher, the following article published in *IEEE Journal of Quantum Electronics*, vol. 46, no. 3, March 2010 is renumbered.

"Laser Dynamics of a 10 GHz 0.55 ps Asynchronously Harmonic Modelocked Er-Doped Fiber Soliton Laser," by Wei-Wei Hsiang, Hon-Chieh Chang, and Yinchieh Lai, DOI 10.1109/JQE.2009.2032559 originally on pp. 292-299 has been renumbered as: pp. 299n – 299u.

Laser Dynamics of a 10 GHz 0.55 ps Asynchronously Harmonic Modelocked Er-Doped Fiber Soliton Laser

Wei-Wei Hsiang, Hon-Chieh Chang, and Yinchieh Lai

***Abstract*—Laser dynamics of a 10 GHz 0.55 ps asynchronously harmonic modelocked Er-doped fiber soliton laser are investigated both theoretically and experimentally. Theoretical analyses based on the master equation model solved by the variational method have indicated that all the pulse parameters of the laser output will exhibit complicated slow periodic variations in the asynchronous soliton modelocking (ASM) mode. New experimental methods based on analyzing directly the RF spectra of the ASM laser output have been developed to accurately determine the sinusoidal variation of the pulse timing and the pulse center wavelength for the first time. It is found that the pulse center wavelength variation can be as large as 1 nm half-peak-to-peak and the pulse timing variation can be as large as 3 ps. The consistency among all the experimental data and theoretical prediction is carefully examined and the results indicate that the ASM pulse dynamics observed experimentally are in good agreement with those obtained from the theoretical analyses.**

***Index Terms*—Asynchronous soliton modelocking, fiber lasers, modelocked lasers, ultrashort optics.**

I. Introduction

ULTRASHORT optical pulse trains with high repetition rates are highly desirable in a wide range of applications including the high speed optical communication [1], ultrafast optical signal processing [2], [3], supercontinuum generation [4], [5], optical frequency metrology [6], and many other scientific researches [7]. Over the past few decades, a lot of efforts have been devoted to the generation of sub-ps pulses with GHz repetition rates from modelocked fiber lasers. In particular, the soliton pulse shaping techniques have been employed in modelocked fiber lasers by active harmonic modelocking [8], hybrid modelocking [4], [9], and passive harmonic modelocking [10], [11]. Recently asynchronous soliton modelocking (ASM) has been proved to be an effective technique of generating ultrashort pulses with GHz repetition rate and high supermode-suppression ratio (SMSR) [12]–[14]. By employing an EO phase modulator driven at the frequency detuned from the cavity harmonic by 10–65 kHz in the modelocked Er-doped fiber laser, 10 GHz 0.8 ps pulses with the SMSR more than 70 dB have been successfully demonstrated [14]. Most interestingly, modelocked fiber lasers with asynchronous phase modulation exhibit many unique laser dynamics when compared to normal actively modelocked fiber lasers. The previous theoretical analyses with the soliton perturbation theory has shown that, due to the asynchronous phase modulation, both the output pulse timing and the output pulse center frequency will exhibit slow sinusoidal variation at a few (or a few tens) kHz [13]. The peak-to-peak displacement of the sinusoidal variation in the pulse center frequency of a 1 GHz 1 ps asynchronously mode-locked Er-doped fiber laser was measured to be 5–25 GHz by using a Fabry–Pérot interferometer [12]. However, the characterization of the pulse timing variation has not been performed experimentally. For practical purposes, it is crucial to carefully characterize such periodic variation of the output pulse parameters before one can actually utilize the ASM fiber lasers in real applications. This is especially true for those applications which will depend on the laser pulse timing or the pulse center frequency.

In the present paper, the laser dynamics of a high-repetition-rate (10 GHz) ultrashort-pulsewidth (0.55 ps) asynchronously harmonic modelocked Er-doped fiber soliton laser are investigated both theoretically and experimentally. Theoretical analyses based on the master equation model solved by the variational method have been carried out. The calculation results indicate that not only the pulse timing and the center frequency, but also all other pulse parameters such as the pulse energy are found to exhibit more complicated slow periodic variations than expected previously. In addition, new experimental techniques have been developed to measure the sinusoidal variations of the pulse timing and the pulse center wavelength accurately. Instead of performing the ultrafast measurement in the time domain, the output pulse timing variation is characterized by analyzing directly the RF spectra of the laser output. The typical half peak-to-peak displacement of the sinusoidal pulse timing variation is identified to be $\sim$3 ps for the studied laser. Furthermore, by measuring the extra pulse timing variation introduced by the pulse center wavelength variation through the group velocity dispersion (GVD) of an external optical fiber section, the corresponding half peak-to-peak displacement of the sinusoidal pulse center wavelength variation can be identified to be $\sim$1 nm. We believe this is for the first time that the variation of these two pulse parameters for an ASM fiber laser is determined accurately from direct experimental data. The connection among the experimental results of the asynchronously modelocked Er-doped fiber laser, including the pulsewidth, the optical spectrum, and the pulse center wavelength variation, are carefully examined. We find that the ASM pulse dynamics observed experimentally are in good agreement with those obtained from the theoretical analyses.

Manuscript received February 13, 2009; revised August 26, 2009. Current version published December 31, 2009. This work was supported in part by the National Science Council of the Republic of China under Contract NSC 96-2628-E-009-154-MY3.

W.-W. Hsiang is with the Department of Physics, Fu Jen Catholic University, Taipei 24205, Taiwan (e-mail: 069179@mail.fju.edu.tw).

H.-C. Chang is with the Department of Photonics, National Chiao-Tung University, Hsinchu 300, Taiwan (e-mail: top1405top@hotmail.com).

Y. Lai is with the Department of Photonics, National Chiao-Tung University, Hsinchu 300, Taiwan, and also with Research Center for Applied Sciences, Academia Sinica, Taipei, 10617 Taiwan (e-mail: yclai@mail.nctu.edu.tw).

Color versions of one or more of the figures in this paper are available online at http://ieeexplore.ieee.org.

Digital Object Identifier 10.1109/JQE.2009.2032559

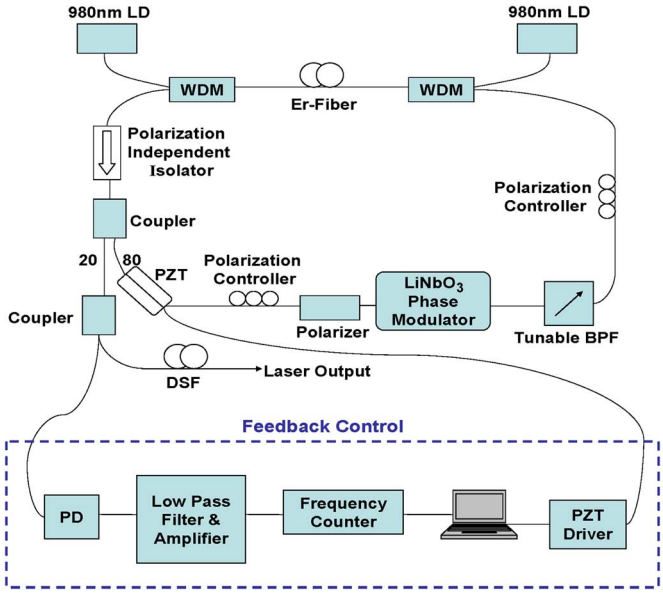

Fig. 1. Schematic of the asynchronously modelocked Er-doped fiber soliton laser and the feedback control module for long-term stabilization. BPF, band-pass filter; PD, photodiode; DSF, dispersion-shift fiber.

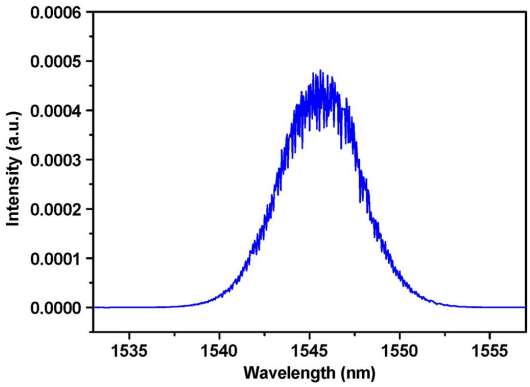

Fig. 2. Optical spectrum of the 10 GHz asynchronously modelocked Er-doped fiber soliton laser.

II. Experimental Setup and Laser Output

The experimental setup of the studied 10 GHz asynchronously harmonic modelocked Er-doped fiber soliton laser is shown in Fig. 1, which is similar to that described in [14], [15]. The modelocked Er-doped fiber laser consists of a $LiNbO_3$ waveguide phase modulator, two polarization controllers, a polarization-insensitive isolator, a polarizer, a tunable optical filter with $\mathrm{FWHM} = 13.5$ nm, a section of 5.5-m Er-doped fiber, an output coupler, two wavelength-division multiplexing (WDM) couplers and two 980-nm pump laser diodes. The average cavity length and GVD are estimated to be 24.8 m and $-4.1\ \mathrm{ps}^2/\mathrm{km}$ respectively. With the suitable orientation of the polarization controllers, stable 10 GHz 0.55 ps pulse trains can be obtained from the laser output when the modulation frequency is detuned from the cavity harmonic frequency by a deviation frequency of 10–65 kHz. Fig. 2 shows the typical optical spectrum of the laser output and the full-width at half-maximum (FWHM) bandwidth of the optical spectrum is 5 nm. The optical frequency components spaced by 0.08 nm

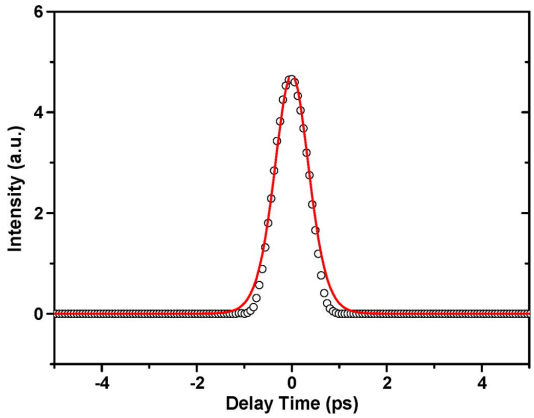

Fig. 3. SHG intensity autocorrelation trace (open circles) and the fitting curve (solid curve) of the laser output, assuming sech^2 pulse shape.

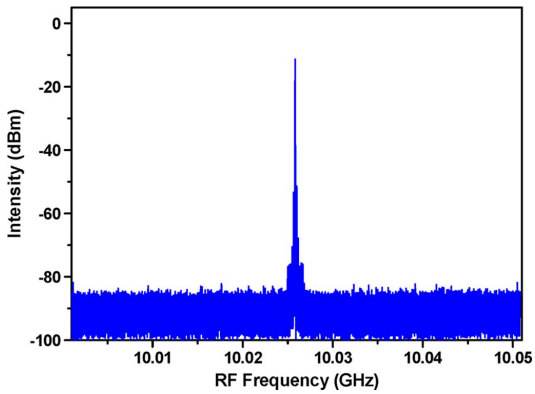

Fig. 4. RF spectrum of the laser output near 10 GHz with 50-MHz span and $\mathrm{SMSR} > 70$ dB.

(i.e., 10 GHz) can be partially resolved by the spectrum analyzer with the resolution bandwidth of 0.07 nm. The corresponding second-harmonic generation (SHG) intensity autocorrelation trace is shown in Fig. 3 by the empty circles. The solid curve in Fig. 3 is the fitting of the SHG intensity autocorrelation trace with the assumption of sech^2 pulse shape, indicating that the pulsewidth is 0.55 ps. The average output power is ~30 mW when the modelocked Er-doped fiber laser is pumped with ~650 mW of pump power. The RF spectrum near 10 GHz from the fast photodiode detecting the laser output is shown in Fig. 4. The span of the RF spectra is 50 MHz and the fundamental cavity frequency of the modelocked Er-doped fiber laser is 8.3 MHz. From the figure, it can be seen that the SMSR is greater than 70 dB at the resolution of 3 kHz, indicating that the main supermode is much larger than the other supermodes. This also means the fast (from ~ MHz to ~ GHz) pulse-to-pulse energy fluctuations, which usually occur in normal harmonic modelocking, can be efficiently suppressed in the asynchronously mode-locked Er-doped fiber laser. The high SMSR also has been confirmed by the uniformity of the10 GHz ASM pulse train measured by a fast sampling oscilloscope, which also suggests that all the pulse slots are filled and there is no multiple-pulse in a time slot [15].

On the RF spectrum we do not observe the beat signals that may be resulted from the supermode hopping. However, since

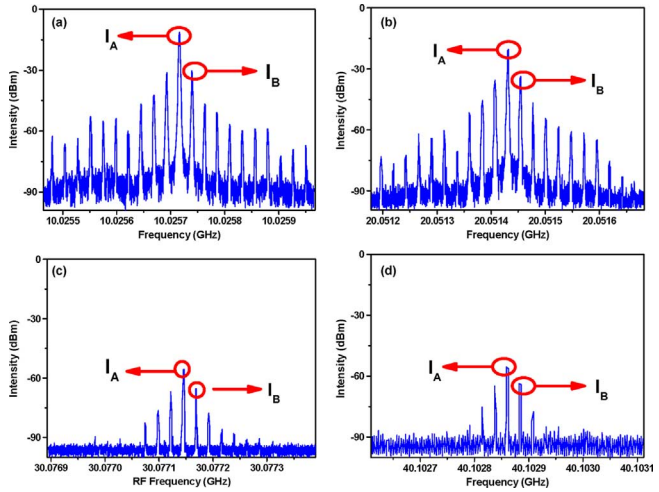

Fig. 5. RF spectra of the laser output with 500 kHz span. Data are taken (a) near 10 GHz; (b) near 20 GHz; (c) near 30 GHz; (d) near 40 GHz.

the fundamental cavity frequency is only 8.3 MHz, it is not easy to make direct observation of the supermode hopping in the optical domain experimentally. The experimental results described above indicate that the advantages of ASM are the shorter pulsewidth and the greater SMSR when compared to normal harmonic mode-locking. The reasons for these advantages can be understood and explained briefly as follows. The combination of the periodic pulse center frequency drift and the fixed optical filter in ASM is equivalent to the effects of sliding-frequency guiding filters in soliton communication systems [16]. The solitons can follow the relative periodic frequency shift induced by asynchronous phase modulation because of their nonlinear optical property and thus the center wavelength of the solitons will oscillate around the spectral peak of the fixed optical filter. On the other hand, the linear noises will experience more losses and will be filtered out more. Hence, the suppression of the supermode noises can be more effective than that of normal frequency modulation (FM) modelocking. Furthermore the suppression of the noises in ASM will also enhance the laser stability for a shorter pulsewidth, which is usually lacked in normal FM modelocking when the pulsewidth is getting shorter and shorter.

In real experiments, the oscillating laser dynamics of ASM fiber lasers can not be observed directly in the optical spectra or the SHG intensity autocorrelation traces due to the long integration time of the two measurements. However, they can be easily observed on the RF spectra of the laser output with a smaller span. Fig. 5 shows the RF spectra of the laser output with a span of 500-kHz near the 10, 20, 30, and 40 GHz pulse train harmonics respectively. The evenly spaced sub-frequency components near the main pulse train harmonics indicate the existence of the slow ($\sim$ kHz) and complicated pulse parameter variation. The similar sub-frequency components also appear near DC, which has been utilized for long-term stabilizing the 10 GHz asynchronously modelocked Er-doped fiber laser [15]. In the following sections, detailed theoretical analyses will be carried out and new measurement methods based on analyzing the RF spectra of Fig. 5 will be developed to fully characterize the pulse dynamics of the ASM fiber laser.

III. Theory of Asynchronous Soliton Modelocking

A. Master Equation of Asynchronous Soliton Modelocking

Under the assumption of small round-trip change, an asynchronously modelocked fiber soliton laser can be described by the master equation as follows [13], [17]:

$$\frac{\partial u(T,t)}{\partial T} = \left(\frac{g_0}{1+\frac{\int |u|^2 dt}{E_s}} - l_0 \right) u + (d_r + j d_i)\frac{\partial^2 u}{\partial t^2} + (k_r + j k_i)|u|^2 u + jM\cos\left[\omega_m (t+RT)\right] u. \quad (1)$$

Here $u(T,t)$ is the complex field envelope of the pulse, g_0 is the unsaturated gain, E_s is the gain saturation energy, l_0 is the linear loss, d_r represents the effect of the optical filtering, d_i is group velocity dispersion, k_r represents the effect of equivalent fast saturable absorption caused by the polarization additive pulse modelocking (P-APM), k_i is the self phase modulation coefficient, M is the phase modulation strength, ω_m is the angular modulation frequency, T is the number of the cavity round trip, t is the time axis measured in the moving frame propagating at a specific group velocity along with the pulse, and R is the linear timing walk-off per round-trip due to asynchronous phase modulation, which can be expressed by

$$R = N\left(\frac{1}{Nf_R} - \frac{1}{f_m}\right) = \frac{\delta f}{f_R f_m}. \quad (2)$$

Here δf is the deviation frequency between the N-th cavity harmonic frequency Nf_R and the modulation frequency f_m. In the following analyses, the sinusoidal modulation curve of the phase modulator will be expanded by the Taylor's series at the center of the pulse $t_0(T)$ to the second order:

$$M\cos\left[\omega_m (t+RT)\right] \approx m_0 - m_1\left[t - t_0(T)\right] - m_2\left[t - t_0(T)\right]^2 \quad (3)$$

where

$$m_1 = M\omega_m \sin\left\{\omega_m\left[t_0(T) + RT\right]\right\} \quad (4)$$

and

$$m_2 = \frac{M}{2}\omega_m^2 \cos\left\{\omega_m\left[t_0(T) + RT\right]\right\}. \quad (5)$$

Such an approximation should be quite accurate since the laser pulsewidth is much shorter than the modulation time period in modelocked fiber lasers.

B. Variational Analysis of Asynchronous Soliton Modelocking

The master equation (1) describing ASM can be reformulated as a variational problem and then solved approximately by assuming a reasonable pulse solution ansatz [18]. In the variational approach, the Lagrangian corresponding to the master equation (1) is

$$\begin{aligned} L = {} & \frac{j}{2}\left(u\frac{\partial u^*}{\partial T} - u^*\frac{\partial u}{\partial T}\right) + d_i\left|\frac{\partial u}{\partial t}\right|^2 - \frac{k_i}{2}|u|^4 \\ & + j d_r\left(\frac{\partial^2 u_0}{\partial t^2}u^* - \frac{\partial^2 u_0^*}{\partial t^2}u\right) \\ & + j\left[k_r|u_0|^2 + (g - l_0)\right](u_0 u^* - u_0^* u) \\ & + \left\{m_1\left(t - t_0(T)\right) + m_2\left(t - t_0(T)\right)^2\right\}(u_0 u^* + u_0^* u) \quad (6) \end{aligned}$$

where $g = g_0/1 + (\int |u|^2 dt/E_s)$ is the saturated gain and the modulation curve has been expanded by (3)–(5). The master equation (1) can de derived from the Lagrange by taking the variation of the functional $I = \int\int L dT dt$ with respective to u and u^*

$$\delta I = \delta \int\int L\left(u, u^*, \frac{\partial u}{\partial T}, \frac{\partial u^*}{\partial T}, \frac{\partial u}{\partial t}, \frac{\partial u^*}{\partial t}\right) dT dt = 0 \quad (7)$$

which is equivalent to the following equation:

$$\frac{\partial L}{\partial u^*} = \frac{\partial}{\partial t}\frac{\partial L}{\partial\left(\frac{\partial u^*}{\partial t}\right)} + \frac{\partial}{\partial T}\frac{\partial L}{\partial\left(\frac{\partial u^*}{\partial T}\right)}. \quad (8)$$

Note that the functions u_0 and u_0^* in (6) are treated like fixed functions so that they do not take part in the variational procedure in (7). However, they should be replaced by u and u^* respectively after performing the variation. This is the standard technique to deal with loss terms under the variational formulation, since all the non-conserved terms can not be directly handled in the usual Lagrangian formulation. For the ASM fiber lasers, the reasonable pulse solution ansatz [17] is given by

$$u(T,t) = a(T)\operatorname{sec} h\left[\frac{t - t_0(T)}{\tau(T)}\right]^{1+j\beta(T)} e^{j[\omega(T)(t-t_0(T))+\theta(T)]} \quad (9)$$

where $a(T)$ is the pulse amplitude, $\tau(T)$ is the pulsewidth, $t_0(T)$ is the pulse timing, $\beta(T)$ is the chirp, $\omega(T)$ is the pulse center frequency, and $\theta(T)$ is the phase. One can obtain the evolution equations of all the pulse parameters from the reduced Lagrange $\langle \mathrm{L} \rangle$

$$\delta \int \langle L \rangle dT = 0 \quad (10)$$

where

$$\langle L \rangle = \int_{-\infty}^{\infty} L_{\mathrm{ansaltz}} dt \quad (11)$$

and L_{ansaltz} represents the Lagrange L in which the ansatz (9) has been substituted for the function u and u^*.

The evolution equations of the pulse parameters are derived from the corresponding Lagrange equations

$$\frac{\partial \langle L \rangle}{\partial x_i} = \frac{\partial}{\partial T}\frac{\partial \langle L \rangle}{\partial\left(\frac{\partial x_i}{\partial T}\right)} \quad (12)$$

where x_i represents each pulse parameter in the ansatz (9). The final derived equations for the pulse center frequency, the timing, the chirp, the amplitude, and the pulsewidth are given below

$$\frac{d\omega}{dT} = -m_1 - \frac{4d_r(1+\beta^2)}{3\tau^2}\omega \quad (13)$$

$$\frac{dt_0}{dT} = 2d_i\omega + 2d_r\beta\omega \quad (14)$$

$$\frac{d\beta}{dT} = \frac{m_2\pi^2\tau^4 + 2a^2\tau^2(k_i - k_r\beta) - 2(2d_i + d_r\beta)(1+\beta^2)}{3\tau^2} \quad (15)$$

$$\frac{da}{dT} = (g - l_0)a + \frac{a\left[8k_r a^2\tau^2 + 6d_i\beta - d_r(\beta^2 + 7 + 9\tau^2\omega^2)\right]}{9\tau^2} \quad (16)$$

$$\frac{d\tau}{dT} = -\frac{4(-2d_r + k_r a^2\tau^2 + 3d_i\beta + d_r\beta^2)}{9\tau} \quad (17)$$

For simplicity the evolution equation for the phase has been omitted because of irrelevance. Please also note that the linear timing drift effects caused by the asynchronous phase modulation are included in the expressions for m_1 and m_2 in (4) and (5), which are periodic functions of T and $t_0(T)$.

C. Periodic Variation of the Pulse Parameters in ASM

The laser dynamics of ASM lasers can be investigated in terms of the evolution of the pulse parameters described by (13)–(17). To the lowest-order approximation, only the evolution of the pulse timing and the pulse center frequency are needed to be considered and the variation of all the other pulse parameters can be ignored. Equations (13) and (14) for chirpless pulse ($\beta = 0$) can be further simplified to the following two equations under the assumption that the oscillating pulse timing $t_0(T)$ is much less than the linear timing drift RT due to asynchronous modulation

$$\frac{d\omega}{dT} = -M\omega_m \sin(\omega_m RT) - \frac{4d_r}{3\tau^2}\omega \quad (18)$$

and

$$\frac{dt_0}{dT} = 2d_i\omega. \quad (19)$$

These two simplified coupled equations can also be derived from the soliton perturbation theory [13]. The solutions of (18) and (19) have the following forms:

$$\omega(T) = \frac{M}{R}\frac{1}{\sqrt{1 + \left(\frac{4d_r}{3\tau^2\omega_m R}\right)^2}}\cos(\omega_m RT + \theta_d) = \Delta\omega\cos(2\pi\delta f T T_R + \theta_d) \quad (20)$$

and

$$t_0(T) = \frac{2d_i M}{\omega_m R^2}\frac{1}{\sqrt{1 + \left(\frac{4d_r}{3\tau^2\omega_m R}\right)^2}}\sin(\omega_m RT + \theta_d) = \Delta t_0 \sin(2\pi\delta f T T_R + \theta_d), \quad (21)$$

where the cavity round-trip time T_R is the inverse of f_R, $\Delta\omega$ and Δt_0 are the half peak-to-peak displacements of the sinusoidal variation in the pulse center frequency and the pulse timing. The two solutions (20) and (21) indicate that to the lowest-order approximation the variation of the pulse timing and the pulse center frequency of ASM lasers is simply sinusoidal at the deviation frequency δf. In addition, the phase difference between the pulse timing and the pulse center frequency is exactly $\pi/2$. This knowledge will be utilized when we try to experimentally determine the pulse center frequency variation in Section IV.

The accurate simulation results of the full set of coupled equations (13)–(17) are shown in Fig. 6. The simulation parameters used are given as follows: $d_i = 0.2$, $d_r = 0.05$, $k_i = 0.4$, $k_r = 0.1$, $g_0 = 4$, $l_0 = 0.8$, $E_0 = 0.47$, $M = 0.8$, $f_R = 8$ MHz, $f_H = 1250\ f_R$, and $\delta f = 25$ kHz. These parameters are estimated by the following procedure. The units for time t

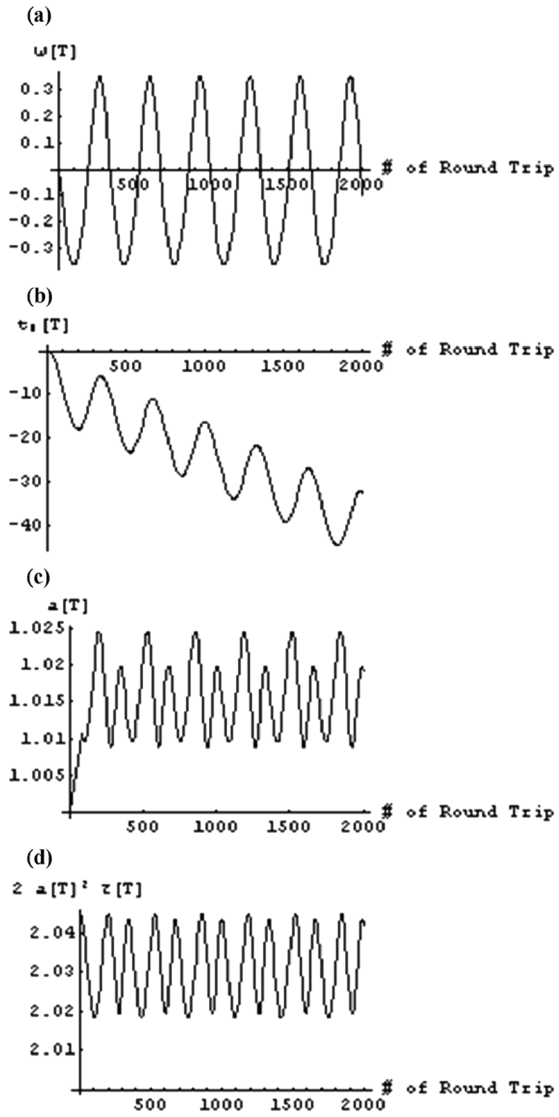

Fig. 6. Slow periodic evolution of the pulse parameters: (a) pulse center frequency; (b) pulse timing; (c) pulse amplitude; (d) pulse energy.

is chosen to be 0.5 ps, which is of the same order with the laser pulsewidth. The value of d_r is then determined from the known filter bandwidth (13.5 nm) and the value of d_i is determined from the estimated cavity average dispersion $(-4.1\ \mathrm{ps}^2/\mathrm{km})$ as well as the cavity length (25 m). The values of l_0 and g_0 are from the roughly estimated loss and gain of the cavity. The values of k_i and k_r are estimated from the values of d_i and d_r under the assumption that the pulse is a chirpless fundamental soliton with roughly the unit normalized pulsewidth and the unit normalized amplitude. To be more specific, we have simply set $k_i = 2d_i$ and required $k_i : k_r = d_i : d_r$ [17]. The value of E_0 also can be estimated based on the above normalization assumption. The other parameters can be directly estimated from the actual experimental conditions. In this way, a reasonable set of parameters that correspond to the studied fiber laser can be obtained for illustrative studies. These numbers should not be very far from the actual operating conditions of the studied laser. From the obtained plots, one can clearly observe the slow periodic variation at the deviation frequency as shown in Fig. 6(a)–(d). The half peak-to-peak displacement of the pulse center frequency variation is found to be ∼125 GHz in Fig. 6(a), corresponding to the variation of the pulse center wavelength of 1 nm around 1550 nm, and the half peak-to-peak displacement of the pulse timing is ∼3 ps in Fig. 6(b). Besides these two parameters, other pulse parameters are also found to exhibit smaller but more complicated slow periodic variation. In particular the evolution of the pulse amplitude and the pulse energy are shown in Fig. 6(c) and (d), respectively, which clearly indicates that the oscillation is not purely sinusoidal and the components of the higher-order harmonics of the deviation frequency appear. Direct numerical simulation of the master equation (1) has also been performed to verify the obtained results. The direct numerical solution is based on the finite difference Crank-Nicholson method for propagating a suitably chosen initial pulse along the T-direction till the stable periodic oscillating solution is reached. The pulse parameters are then extracted from the numerical pulse solution for comparison. The ASM oscillating behavior is directly observed and the excellent agreement with the variational solution has been found. Nevertheless, even though the variational approach as well the direct numerical solution have been proved to be very helpful for understanding the steady-state dynamics of ASM modelocked fiber lasers, they are both under the assumptions of the master equation model (1). In particular, the cavity round-trip change has been assumed to be small, only the evolution of a single pulse is considered, and no noise source is included. Therefore, to investigate the noise dynamics of ASM modelocked fiber lasers will require a more elaborated theoretical model and will be a good subject of further studies.

IV. Experimental Determination of Periodic Variation of the Pulse Parameters

According to the results obtained from the theoretical analyses in Section III, all the pulse parameters of the ASM laser may exhibit the slow periodic variation. We have found that when the modulation depth of the phase modulator is not too large, the simulation results indicate that the variation appearing in the pulse timing and the pulse center frequency are nearly pure sinusoidal at the deviation frequency δf. In this section, new experimental methods based on directly analyzing the RF spectra of the laser output are developed to directly characterize the sinusoidal variation of the pulse timing and pulse center frequency.

A. New Method to Determine the Sinusoidal Variation of Pulse Timing

With the reasonable assumption that the pulse timing variation is mainly a simple sinusoidal function at the deviation frequency δf, the photocurrent from the fast photodiode detecting the pulse train can be expressed by

$$i(t) = [r(t) \otimes p(t)] \otimes \sum_{m=-\infty}^{m=\infty} \delta\left[t - mT_H + \Delta t_0 \sin(2\pi \delta f m T_H)\right] \tag{22}$$

where $r(t)$ is the response function of the fast photodiode, $p(t) = |u(t)|^2$ is the pulse intensity, $T_H = 1/f_H = 1/Nf_R$ is the period of the cavity harmonic, Δt_0 is the half peak-to-peak

displacement of the sinusoidal pulse timing variation, $\delta(\cdot)$ is the Dirac's delta function, and $\otimes$ stands for the operation of convolution. We have assumed that the variation of other pulse parameters can be ignored at least to the first order approximation. This should be a reasonable assumption given with the theoretical results in Section III, where the variation of the pulse energy is much smaller in percentage. The Fourier transform of the photocurrent $i(t)$ can be expressed as

$$I(\omega) \propto R(\omega)P(\omega) \sum_{m=-\infty}^{m=\infty} \sum_{n=-\infty}^{n=\infty} J_n(\omega \Delta t_0) \times \delta(\omega - 2\pi m f_H - 2\pi n \delta f) \quad (23)$$

where $R(\omega)$ and $P(\omega)$ are the Fourier transforms of the response function of the fast photodiode and the pulse intensity distribution, respectively, and $J_n(\cdot)$ is the Bessel function of the first kind of order n. The periodic Dirac's delta functions with the sinusoidal timing variation in the time domain gives rise to the comb-like sub-components in the frequency domain as shown in Fig. 5. That is, the pure sinusoidal timing variation will produce the frequency components with the amplitudes of $J_n(\omega \Delta t_0)$, which are spaced equally by the deviation frequency δf around the pulse train harmonics $m f_H$. When the pulsewidth is sub-ps short and the response speed of the photodiode is also fast enough compared to the slow modulation frequency, then the intensity of the n-th sub-component of $I(\omega)$ in (23) is simply proportional to $|J_n(\omega \Delta t_0)|^2$. Therefore, by comparing the peak intensity at the main pulse train harmonic $(\mathrm{n} = 0)$ to the peak intensity at the first sub-component $(\mathrm{n} = 1)$ from the experimental data,

$$\Delta = \left| \frac{J_0[2\pi m f_H \Delta t_0]}{J_1[2\pi (m f_H + \delta f) \Delta t_0]} \right|^2 \quad (24)$$

the half peak-to-peak displacement Δt_0 of the sinusoidal pulse timing variation can be identified.

B. Experimental Determination of the Pulse Timing Variation by Analyzing the RF Spectra of Laser Output

Experimentally the peak intensity ratio Δ in (24) can be obtained directly by analyzing the RF spectra of the laser output. The output pulse train from the 10 GHz asynchronously modelocked Er-doped fiber soliton laser is detected by a fast photodiode and the amplified electric signals of the photodiode are connected to a RF spectrum analyzer. The RF spectra with a smaller span of 500 kHz near the 10 GHz, 20 GHz, 30 GHz, and 40 GHz of the main pulse train harmonics have been shown in Fig. 5(a)–(d), respectively. The values of the RF peak intensities I_A at $m f_H$ and I_B at $m f_H + \delta f$ for $\mathrm{m} = 1$ to $\mathrm{m} = 4$ are represented by the solid squares in Fig. 7. According to (24), the differences between I_A and I_B are equal to

$$\begin{aligned} I_A - I_B &= 10 \log_{10} \Delta \\ &= 20 \log_{10} \left(\left| \frac{J_0[2\pi m f_H \Delta t_0]}{J_1[2\pi (m f_H + \delta f) \Delta t_0]} \right| \right) \\ &\approx 20 \log_{10} \left(\left| \frac{J_0[2\pi m f_H \Delta t_0]}{J_1[2\pi m f_H \Delta t_0]} \right| \right). \end{aligned} \quad (25)$$

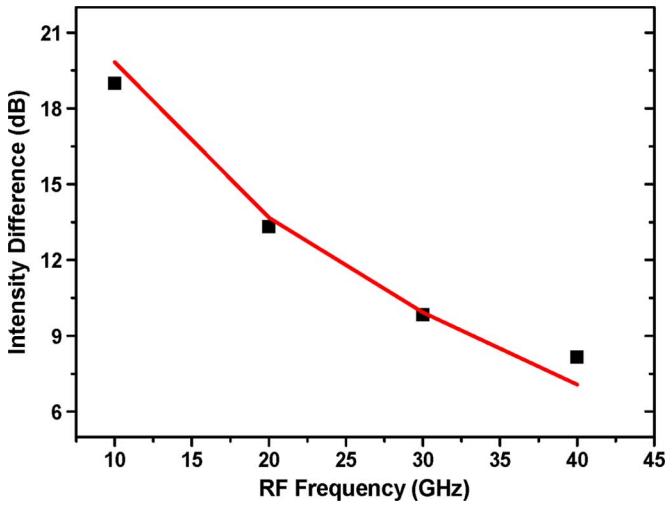

Fig. 7. Intensity difference between the 0th and 1st frequency sub-components around the 10, 20, 30, 40 GHz pulse train harmonic frequencies.

The fitting curve based on (25) shown by the solid line is used to identify the value of the half peak-to-peak displacement of the sinusoidal pulse timing variation Δt_0. The value is found to be around 3.5 ps for all the four values of m. The consistency of the estimated values from different orders of pulse train harmonics indicates that the proposed method should be able to give consistent and reasonable results for the pulse timing variation.

C. New Method to Identify Sinusoidal Variation of Pulse Center Frequency

The method developed above for determining the pulse timing variation can be further extended to identify the pulse center frequency (wavelength) variation as well. The pulse center wavelength variation will turn into extra pulse timing variation after the pulse train of ASM propagates through an external section of dispersive optical fiber. As indicated by (20) and (21), the phase difference between the two sinusoidal variations of the pulse timing and the pulse center frequency is $\pi/2$, i.e., sine and cosine, respectively. Thus, the variation of the pulse timing $\Delta t_1(T)$ of the ASM pulse train after propagating through a length L of the optical fiber with the dispersion parameter D will be given by

$$\begin{aligned} \Delta t_{tot}(T) &= \Delta t_0 \sin(RT) + \Delta\lambda DL \cos(RT) \\ &= \sqrt{(\Delta t_0)^2 + (\Delta\lambda DL)^2} \sin(RT + \phi) \\ &= \Delta t_1 \sin(RT + \phi) \end{aligned} \quad (26)$$

where $\Delta\lambda DL \cos(RT)$ is the extra pulse timing variation introduced by the dispersion of the external optical fiber. Based on (26), the half peak-to-peak displacement of the pulse center wavelength variation $\Delta\lambda$ can be determined according to

$$\Delta\lambda = \frac{\sqrt{\Delta t_1^2 - \Delta t_0^2}}{DL} \quad (27)$$

with the additional experimental measurement for Δt_1.

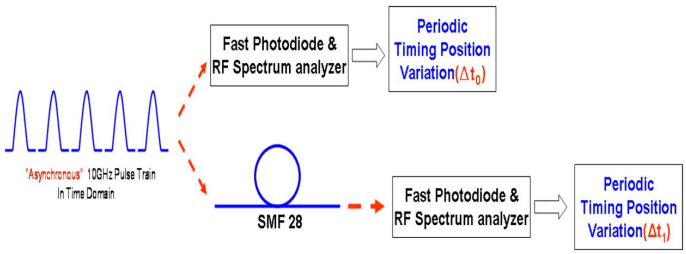

Fig. 8. Experimental setup for the measurement of the pulse center frequency variation.

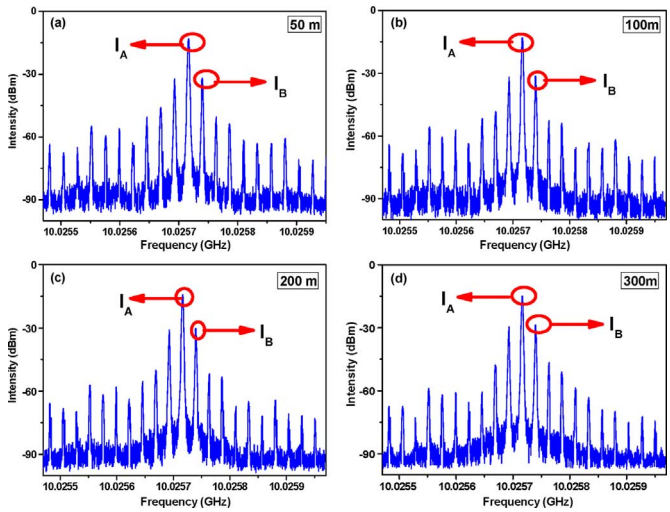

Fig. 9. RF spectra of the pulse train after propagating through an external section of SMF-28 fiber. The data are taken near 10 GHz with 500-kHz span. The fiber length is (a) 50 m; (b) 100 m; (c) 200 m; (d) 300 m.

D. Experimental Examination of the Pulse Center Frequency

The experimental setup used to measure the sinusoidal variation of the pulse center wavelength is shown in Fig. 8. As the same as the measurement of the pulse timing variation, the analyses of RF spectra of the laser output are utilized to identify the pulse timing variation before and after (i.e., Δt_0 and Δt_1) the pulse train propagates through an external single mode fiber. Fig. 5(a) and Fig. 9(a)–(d) are the RF spectra of the pulse train measured near 10 GHz with a 500-kHz span before and after propagating through 50-m, 100-m, 200-m, and 300-m SMF-28 fibers, respectively. It can be clearly seen that the peak intensity ratio between the 0th and 1st sub-frequency components is indeed reduced with increasing fiber length. By comparing the differences of the RF intensities I_A and I_B, the corresponding pulse timing variations Δt_0 and Δt_1 are evaluated according to (25) and represented by the solid squares in Fig. 10. The curve in Fig. 10 is the fitting curve of Δt_1 in (26) with the parameter $D = 17\ \mathrm{ps}^2/\mathrm{km}$ for the SMF-28 fiber. The fitting results indicate that the half peak-to-peak displacement of the sinusoidal pulse center wavelength variation $\Delta\lambda$ is around 1.12 nm for the studied ASM laser.

V. Discussion

The ASM laser dynamics have been analyzed theoretically in Section III and investigated experimentally in Section IV.

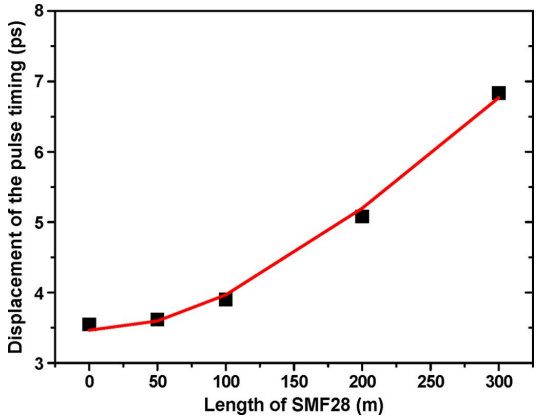

Fig. 10. Measurement (square dots) and the fitting curve (solid line) of the net pulse timing variation Δt_1 versus the length of the SMF-28 fiber.

Although the slow periodic variation of the pulse center frequency and the pulse timing do not appear directly in the experimental optical spectra and SHG autocorrelator traces presented in Section II, the connection among all the experimental and theoretical results still needs to be carefully checked for ensuring consistency. According to the SHG autocorrelator trace in Section II, the measured pulsewidth is 0.55 ps. For such a pulsewidth, the corresponding transform-limited optical FWHM bandwidth λ_{FWHM} is 4.58 nm with the assumption of the sech^2 pulse shape. Compared to the measured optical spectrum of the pulses presented in Section II, it implies that an extra ~0.5 nm bandwidth is introduced by the slow periodic variation of the pulse center wavelength. Theoretically the broadened optical spectrum caused by the sinusoidal pulse center wavelength variation can be estimated by calculating the averaged optical spectrum

$$\delta f \int_0^{\frac{1}{\delta f}} \mathrm{sec}\, h^2 \left(\frac{\lambda - (\lambda_0 + \Delta\lambda \cos(2\pi\delta f T_v))}{\lambda_{\mathrm{FHWM}}} \right) dT_v. \qquad (28)$$

By using $\lambda_{\mathrm{FHWM}} = 4.58$ nm derived form the pulsewidth and $\Delta\lambda = 1.12$ nm obtained from Section IV, the calculated FWHM bandwidth of the broadened optical spectrum from (28) is close to that measured by the optical spectrum analyzer. This shows that the results obtained from Sections II–IV are consistent and also proves the feasibility of the new measurement techniques for identifying the pulse timing variation and the pulse center frequency variation presented in Section IV.

VI. Conclusion

To conclude, the pulse dynamics of a 10 GHz 0.55 ps asynchronously mode-locked Er-doped fiber soliton lasers have been carefully investigated both theoretically and experimentally. By putting the experimental parameters of the studied mode-locked Er-doped fiber laser into the theoretical formulation, the simulation results have shown that all the ASM pulse parameters will exhibit complicated slow periodic variation. In order to know more exactly the magnitudes of the sinusoidal variation for the ASM pulse timing as well as the pulse center wavelength, new experimental methods based on analyzing the RF spectra of the

laser output have been developed. The consistency of all the experimental and theoretical results has been examined and verified. The ASM laser dynamics observed experimentally have been found to be in good agreement with the results obtained from the theoretical analyses. The evolution equations of the pulse parameters derived from the variational analysis should provide a very illustrative physical model for understanding the laser dynamics of ASM fiber lasers.

REFERENCES

[1] M. Nakazawa, H. Kubota, K. Suzuki, E. Yamada, and A. Sahara, "Ultra-high speed and long-distance TDM and WDM soliton transmission technology," *IEEE J. Sel. Topics Quantum Electron.*, vol. 6, no. 2, pp. 363–396, Mar./Apr. 2000.

[2] J. P. Wang, B. S. Robinson, S. A. Hamilton, and E. P. Ippen, "Demonstration of 40-Gb/s packet routing using all-optical header processing," *IEEE Photon. Technol. Lett.*, vol. 18, no. 21, pp. 2275–2277, Nov. 2006.

[3] Y. Miyoshi, K. Ikeda, H. Tobioka, T. Inoue, S. Namiki, and K. Kitayama, "Ultrafast all-optical logic gate using a nonlinear optical loop mirror based multi-periodic transfer function," *Opt. Exp.*, vol. 16, pp. 2570–2577, 2008.

[4] C. X. Yu, H. A. Haus, E. P. Ippen, W. S. Wong, and A. Sysoliatin, "Gigahertz-repetition-rate mode-locked fiber laser for continuum generation," *Opt. Lett.*, vol. 25, pp. 1418–1420, 2000.

[5] G. T. Nogueira and F. C. Cruz, "Efficient 1 GHz Ti:sapphire laser with improved broadband continuum in the infrared," *Opt. Lett.*, vol. 31, pp. 2069–2071, 2006.

[6] A. Bartels, R. Gebs, M. S. Kirchner, and S. A. Diddams, "Spectrally resolved optical frequency comb from a self-referenced 5 GHz femtosecond laser," *Opt. Lett.*, vol. 32, pp. 2553–2555, 2007.

[7] C. X. Yu, H. A. Haus, and E. P. Ippen, "Soliton squeezing at the gigahertz rate in a Sagnac loop," *Opt. Lett.*, vol. 26, pp. 669–671, 2001.

[8] M. Nakazawa and E. Yoshida, "A 40-GHz 850-fs regeneratively FM mode-locked polarization-maintaining erbium fiber ring laser," *IEEE Photon. Technol. Lett.*, vol. 12, no. 12, pp. 1613–1615, Dec. 2000.

[9] M. Margalit, C. X. Yu, S. Namiki, E. P. Ippen, and H. A. Haus, "Harmonic mode locking using regenerative phase modulation," *IEEE Photon. Technol. Lett.*, vol. 10, no. 3, pp. 337–339, Mar. 1998.

[10] J. N. Kutz, B. C. Collings, K. Bergman, and W. H. Knox, "Stabilized pulse spacing in soliton lasers due to gain depletion and recovery," *IEEE J. Quantum Electron.*, vol. 34, no. 9, pp. 1749–1757, Sep. 1998.

[11] S. Zhou, D. G. Ouzounov, and F. W. Wise, "Passive harmonic modelocking of a soliton Yb fiber laser at repetition rates to 1.5 GHz," *Opt. Lett.*, vol. 31, pp. 1041–1043, 2006.

[12] C. R. Doerr, H. A. Haus, and E. P. Ippen, "Asynchronous soliton mode locking," *Opt. Lett.*, vol. 19, pp. 1958–1960, 1994.

[13] H. A. Haus, D. J. Jones, E. P. Ippen, and W. S. Wong, "Theory of soliton stability in asynchronous modelocking," *J. Lightw. Technol.*, vol. 14, no. 4, pp. 622–627, Apr. 1996.

[14] W.-W. Hsiang, C.-Y. Lin, M.-F. Tien, and Y. Lai, "Direct generation of a 10 GHz 816 fs pulse train from an erbium-fiber soliton laser with asynchronous phase modulation," *Opt. Lett.*, vol. 30, pp. 2493–2495, 2005.

[15] W.-W. Hsiang, C. Lin, N. Sooi, and Y. Lai, "Long-term stabilization of a 10 GHz 0.8 ps asynchronously mode-locked Er-fiber soliton laser by deviation-frequency locking," *Opt. Exp.*, vol. 14, pp. 1822–1828, 2006.

[16] L. F. Mollenauer, J. P. Gordon, and S. G. Evangelides, "The sliding-frequency guiding filter: An improved form of soliton jitter control," *Opt. Lett.*, vol. 17, pp. 1575–1577, 1992.

[17] H. A. Haus, J. G. Fujimoto, and E. P. Ippen, "Structures for additive pulse mode locking," *J. Opt. Soc. Amer. B*, vol. 8, pp. 2068–2076, 1991.

[18] D. Anderson, "Variational approach to nonlinear pulse propagation in optical fibers," *Phys. Rev. A*, vol. 27, pp. 3135–3145, 1983.

Wei-Wei Hsiang received the B.S. degree in telecommunication engineering the M.S. and Ph.D. degrees in electro-optical engineering from National Chiao-Tung University, Taiwan, in 1996, 1998, and 2006, respectively.

He joined the Department of Physics at the Fu Jen Catholic University, Taiwan, in 2006, as an Assistant Professor. His research interests include modelocked fiber lasers and ultrafast nonlinear optics.

Hon-Chieh Chang received the B.S. degree in electrical engineering from I-Shou University, Taiwan, in 2006 and the M.S. degree in electro-optical engineering from National Chiao-Tung University, Taiwan, in 2008.

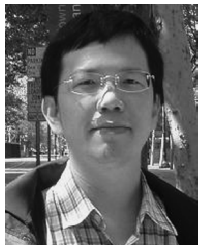

Yinchieh Lai received the B.S. degree in electrical engineering from National Taiwan University, Taiwan, in 1985 and the M.S. and Ph.D. degrees in electrical engineering from Massachusetts Institute of Technology (MIT), Cambridge, in 1989 and 1991, respectively.

He joined the Faculty of the Institute of Electro-Optical Engineering at the National Chiao-Tung University, Taiwan in 1991, where he is now a Professor. His main research directions include quantum nonlinear optical pulse propagation, nonlinear optics, modelocked fiber lasers, and fiber devices.